Biochimica et Biophysica Acta 1822 (2012) 1617–1628

Contents lists available at SciVerse ScienceDirect

Biochimica et Biophysica Acta

journal homepage: www.elsevier.com/locate/bbadis

Proteolytic cleavage of the disease-related lysosomal membrane glycoprotein CLN7

Pieter Steenhuis [a], Joshua Froemming [a], Thomas Reinheckel [b], Stephan Storch [a,*]

[a] Department of Biochemistry, Children's Hospital, University Medical Center Hamburg-Eppendorf, D-20246 Hamburg, Germany
[b] Institute of Molecular Medicine and Cell Research and BIOSS Centre for Biological Signalling Studies, Albert-Ludwigs University Freiburg, D-79104 Freiburg, Germany

ARTICLE INFO

Article history:
Received 12 January 2012
Received in revised form 8 May 2012
Accepted 29 May 2012
Available online 2 June 2012

Keywords:
CLN7/MFSD8
Cathepsin L
Proteolytic cleavage
Lysosomal storage disorder
Neurodegeneration

ABSTRACT

CLN7 is a polytopic lysosomal membrane glycoprotein of unknown function and is deficient in variant late infantile neuronal ceroid lipofuscinosis. Here we show that full-length CLN7 is proteolytically cleaved twice, once proximal to the used *N*-glycosylation sites in lumenal loop L9 and once distal to these sites. Cleavage occurs by cysteine proteases in acidic compartments and disruption of lysosomal targeting of CLN7 results in inhibition of proteolytic cleavage. The apparent molecular masses of the CLN7 fragments suggest that both cleavage sites are located within lumenal loop L9. The known disease-causing mutations, p.T294K and p.P412L, localized in lumenal loops L7 and L9, respectively, did not interfere with correct lysosomal targeting of CLN7 but enhanced its proteolytic cleavage in lysosomes. Incubation of cells with selective cysteine protease inhibitors and expression of CLN7 in gene-targeted mouse embryonic fibroblasts revealed that cathepsin L is required for one of the two proteolytic cleavage events. Our findings suggest that CLN7 is inactivated by proteolytic cleavage and that enhanced CLN7 proteolysis caused by missense mutations in selected luminal loops is associated with disease.

1. Introduction

Lysosomal membrane proteins have numerous functions including acidification of the lysosomal lumen, mediating fusion with other organelles, self-protection against proteolytic digestion, export of degradation products into the cytosol, protein import from the cytosol and motion of organelles [1]. The precise functions, however, of the majority of the lysosomal membrane proteins are unknown [2,3]. Defects in genes encoding lysosomal membrane proteins have been linked to a growing number of lysosomal storage disorders [4]. The neuronal ceroid lipofuscinoses (NCL) represent a group of lysosomal storage diseases which are characterized by the accumulation of lipofuscin-like ceroid lipopigments and the selective damage and loss of neurons [5]. NCL-causing mutations have been identified in eleven different genes encoding the soluble cysteine-string protein alpha (CLN4/DNAJC5), soluble lysosomal proteins (CLN1/palmitoyl-protein thioesterase 1, CLN2/tripeptidyl peptidase I, CLN5 and CLN10/cathepsin D), lysosomal membrane proteins (CLN3, CLN7/MFSD8, CLN12/ATP13A2 and ClC-7) and polytopic membrane proteins localized in the endoplasmic reticulum (CLN6 and CLN8) [5–8]. CLN7 disease, late infantile variant phenotype (MIM# 610951) is caused by defects in the *CLN7/MFSD8* gene with 31 different mutations known to date [9–14]. The *CLN7/MFSD8* gene encodes a polytopic lysosomal membrane protein of unknown function with 12 transmembrane domains, cytosolic N and C termini and two confirmed *N*-glycosylation sites in positions N371 and N376 [15]. The *CLN7/MFSD8* gene product is localized in lysosomes in non-neuronal and neuronal cells [9,15,16]. Its lysosomal targeting along the indirect pathway via the plasma membrane is mediated by an N-terminal dileucine-based E^{9} QEP $L^{13}L^{14}$ sorting signal [15]. CLN7 is a member of the major facilitator superfamily (MFS) of transporter proteins which are capable of transporting a wide range of low-molecular-mass substrates including carbohydrates and amino acids [17]. CLN7 is therefore believed to be a lysosomal transporter, but its substrate has not been identified.

We have previously shown that the intensity of CLN7-GFP immunoreactive bands increased after inhibiting cysteine and aspartic proteases [15]. In the present study we describe the proteolytic cleavage of the CLN7 membrane protein in endosomal/lysosomal compartments. CLN7 is asymmetrically cleaved twice in a cell-type independent manner. Inhibitor studies and expression analyses in gene-targeted mouse embryonic fibroblasts (MEF) demonstrated that the cysteine protease cathepsin L (Ctsl) is required for one of the two proteolytic cleavage

Abbreviations: BFA, brefeldin A; CHX, cycloheximide; Ctsb, cathepsin B; Ctsl, cathepsin L; DMEM, Dulbecco's minimal essential medium; endo H, endoglycosidase H; ER, endoplasmic reticulum; GFP, green fluorescent protein; HEK293, human embryonic kidney 293; HGSNAT, heparin sulfate acetyl-CoA α-glucosaminide N-acetyltransferase; IC50, half maximal inhibitory concentration; LAP, lysosomal acid phosphatase; MEF, mouse embryonic fibroblast; MFS, major facilitator superfamily; ML1, mucolipin-1; NCL, neuronal ceroid lipofuscinosis; PNGase F, peptide:*N*-glycosidase F; TLR9, Toll-like receptor 9; TM, transmembrane domain; vLINCL, variant late-infantile NCL

* Corresponding author at: Department of Biochemistry, Children's Hospital, University Medical Center Hamburg-Eppendorf, Martinistrasse 52, Building N27, D-20246 Hamburg, Germany. Tel.: +49 40 7410 51967; fax: +49 40 7410 58504.
E-mail address: storch@uke.uni-hamburg.de (S. Storch).

0925-4439/$ – see front matter © 2012 Elsevier B.V. All rights reserved.
doi:10.1016/j.bbadis.2012.05.015

events. In addition, two missense mutations identified in patients with CLN7 disease, p.T294K and p.P412L, resulted in increased proteolytic cleavage of CLN7 in lysosomes.

2. Materials and methods

2.1. Antibodies and reagents

The following antibodies were used for Western blot analyses: mouse anti-GFP (1:500 dilution; Roche Applied Science, Mannheim, Germany), mouse anti-FLAG (clone M2, 1:1000 dilution; Sigma-Aldrich, Taufkirchen, Germany), and mouse anti-Myc (clone 9B11, 1:1000 dilution; Cell Signaling Technologies, Danvers, MA). Antibodies used for immunofluorescence microscopy were as follows: polyclonal anti-human cathepsin D (1:100 dilution, [18]), monoclonal anti-human LAMP-1 (clone H4A3, 1:150 dilution; Developmental Studies Hybridoma Bank, Iowa City, IA), polyclonal anti-Myc (1:100 dilution; Sigma-Aldrich), monoclonal anti-FLAG (clone M2, 1:100 dilution) and polyclonal anti-FLAG (1:100 dilution, Sigma-Aldrich). Secondary goat anti-mouse antibodies coupled to horse radish peroxidase were from Dianova (Hamburg, Germany) and were used at a 1:5000 dilution. Fluorochrome-coupled secondary antibodies goat anti-rabbit IgG AlexaFluor 488, goat anti-rabbit IgG Cy5, goat anti-rabbit IgG AlexaFluor 546, goat anti-mouse IgG AlexaFluor 488 and goat anti-mouse IgG AlexaFluor 546 were from Invitrogen (Karlsruhe, Germany) and used at a 1:1000 dilution.

The following reagents were obtained commercially as indicated: Normocin from Invivogen (San Diego, CA), fast digest restriction enzymes from Fermentas (St. Leon-Rot, Germany), Quick Start Bradford Protein Assay from Bio-Rad (Munich, Germany), peptide *N*-glycosidase F (PNGase F) from Roche Applied Sciences (Mannheim, Germany), endoglycosidase H (endo H) from New England Biolabs (Ipswich, MA), Pfu Turbo polymerase and QuikChange site-directed mutagenesis kit from Stratagene Europe (Amsterdam, the Netherlands), Dulbecco's minimal essential medium (DMEM), fetal calf serum, Glutamax, penicillin, streptomycin, trypsin/EDTA, Lipofectamine 2000 and Optimem from Invitrogen, Phusion® High-Fidelity DNA polymerase from Finnzymes (Espoo, Finland), GeneJET™ Plasmid Mini Kit and gel extraction kit from Fermentas (St. Leon-Rot, Germany), Plasmid Midi Kit from QIAGEN (Hilden, Germany), medium for cultivating *Escherichia coli* from Roth (Karlsruhe, Germany), prestained Rainbow marker, and ultrapure dNTPs from GE Healthcare Life Sciences (Freiburg, Germany). Oligonucleotides used for cloning and sequencing were synthesized by MWG Biotech (Munich, Germany). Cycloheximide, brefeldin A, leupeptin, pepstatin A, E-64, SID26681509, and protease inhibitor cocktail were purchased from Sigma-Aldrich, Ctsl inhibitor Z-FY-CHO from Calbiochem (Nottingham, UK), Albumin standard and enhanced chemiluminescence reagents from Thermo Fisher Scientific (Rockford, IL). GFP-TRAP® agarose beads were purchased from ChromoTek (Planegg-Martinsried, Germany).

2.2. Plasmids and transgenic cDNA constructs

The generation of the GFP-CLN7 cDNA construct has been described previously [15]. A cDNA construct with a triple FLAG tag fused to the N-terminus of CLN7 was generated by amplifying the cDNA coding for human CLN7 (NM_152778, RZPD clone IRATp970E0532D6; imaGenes, Berlin, Germany) by PCR using primers 3xFLAG pCMV10-CLN7 F/R and by cloning the resulting PCR product into *Hind*III and *Bam*HI sites of expression vector p3xFLAG-CMV10 (Sigma-Aldrich). The pcDNA3.1 (+) CLN7-3xMyc cDNA construct was generated by amplifying a PCR product with primers pcDNA3.1. (+) CLN7-3xMyc F/R using GFP-CLN7 as a DNA template. The resulting PCR product was subcloned into the pCR®-BluntII-TOPO® vector (Invitrogen), the fragment subsequently excised with restriction enzymes *Hind*III and *Bam*HI and cloned into the corresponding sites of expression vector pcDNA3.1 Hygro (+)-3xMyc [19]. The GFP-CLN7-3xMyc expression construct was generated by amplifying a PCR product with primers pcDNA3.1 GFP-CLN7 3xMyc F/R using the GFP-CLN7 cDNA as template. The PCR product was cloned into pcDNA3.1D/V5-His-TOPO® vector (Invitrogen). For the cloning of the 3xFLAG-mucolipin-1 construct a cDNA clone (IMAGE clone p998L049490Q) containing the human mucolipin-1 cDNA (NM_020533) was amplified by PCR with primers 3xFLAG pCMV10-mucolipin-1F/R. The resulting PCR product was subcloned into the pCR®-BluntII-TOPO® vector and recombinant vectors were subsequently incubated with restriction enzymes *Hind*III and *Sac*I. The fragment was finally cloned into the *Hind*III/*Sac*I sites of vector pCMV10 3xFLAG (Sigma).

All primers used for cloning and site-directed mutagenesis are described in the Supplementary material (Table S1). Mutagenesis was performed using the QuikChange® site-directed mutagenesis kit. All constructs were sequenced by Seqlab (Göttingen, Germany). The cDNAs encoding mouse cathepsin L (Ctsl, NM_009984) and cathepsin B (Ctsb, NM_007798) cloned into expression vector pcDNA3.1 (+) were kindly provided by Dr. Schröder (University of Kiel, Germany).

2.3. Cell culture and transfections

COS-7, HEK293 cells, wild-type and $Ctsl^{(-/-)}$- and $Ctsb^{(-/-)}$ mouse embryonic fibroblasts (MEF) were cultivated in DMEM containing 10% fetal calf serum, 1× Glutamax, 100 µg/ml Normocin, 100 IU/ml penicillin, and 50 mg/ml streptomycin. $Ctsb^{(-/-)}$ and $Ctsl^{(-/-)}$ MEF were described previously [20,21]. Cells were transfected with Lipofectamine 2000 (Invitrogen) and Optimem according to the manufacturers' instructions and cells were analyzed 24 h after the start of transfection. Where indicated, media were supplemented with brefeldin A (BFA) or protease inhibitors during the complete course of transfection.

2.4. Western blotting

Cells grown on 35 mm dishes were scraped in ice-cold phosphate-buffered saline, pH 7.4, and centrifuged for 5 min at 1000×*g*. Cell pellets were lysed in 100 µl ice-cold lysis buffer (10 mM Tris pH 7.5, 150 mM NaCl, 5 mM EDTA, 0.1% SDS, 1% TX-100, 1% sodium deoxycholate) supplemented with protease inhibitors. After incubation for 30 min on ice, extracts were centrifuged at 15,000×*g* for 10 min followed by determination of protein concentrations with a Bradford assay. Aliquots of total cell extracts were solubilized in Laemmli sample buffer containing 1% beta-mercaptoethanol at 50 °C for 10 min. Samples were separated by SDS-PAGE (10% acrylamide unless otherwise specified). Proteins were transferred to PVDF membranes (GE Healthcare, Munich, Germany). ECL-detection was performed using the manufacturer's instructions (Thermo Fisher Scientific) and blots were imaged on a Molecular Imager (Model Chemi Doc XRS, Bio-Rad). For complete removal of all *N*-linked oligosaccharides from CLN7 50 µg of total cell extracts was denatured for 10 min at 50 °C in 0.3% SDS and protease inhibitors, followed by the addition of NP-40 (final concentration: 1%) and 3 units PNGase F. For removal of *N*-linked high-mannose and hybrid oligosaccharides 50 µg of total cell extracts was denatured in denaturation buffer (New England Biolabs) for 10 min at 50 °C, followed by the addition of buffer G5 and 1000 units endo H. Samples were incubated in the presence of endo H or PNGase at 37 °C for 30 to 60 min, followed by analysis by SDS-PAGE and immunoblotting.

2.5. Co-immunoprecipitations

HEK293 cells were co-transfected with GFP-CLN7 and 3xFLAG-CLN7 or GFP-CLN7 and CLN7-3xMyc and harvested 24 h after the start of transfection. Cell pellets were lysed using 200 µl of a low-detergent lysis buffer (10 mM Tris pH 7.5, 150 mM NaCl, 5 mM EDTA, 0.5% NP40, protease inhibitors) to leave protein complexes intact. Subsequently, GFP-CLN7

was precipitated using GFP-TRAP®. Lysates were adjusted to 500 µl with dilution buffer (10 mM Tris pH 7.5, 150 mM NaCl, 5 mM EDTA, protease inhibitors), pre-cleared with empty agarose beads for 1 h at 4 °C and subsequently incubated with GFP-TRAP® agarose beads for 2 h at 4 °C. Beads were washed once with 500 µl dilution buffer without protease inhibitors and co-precipitated 3xFLAG-CLN7 and CLN7-3xMyc were eluted in Laemmli sample buffer containing 1% beta-mercaptoethanol at 50 °C for 10 min. To confirm successful immunoprecipitation, GFP-CLN7 was eluted from a small fraction (10%) of the beads in Laemmli sample buffer containing 1% beta-mercaptoethanol at 95 °C for 10 min. The eluted fractions were analyzed by Western blotting.

2.6. Cycloheximide pulse-chase analysis

COS-7 cells were transiently transfected for 24 h and were either harvested (pulse) or incubated in the presence of 100 µg/ml cycloheximide (CHX) to stop new protein synthesis for the indicated time intervals. Total cell extracts were analyzed by SDS-PAGE and anti-FLAG immunoblotting.

2.7. Immunofluorescence confocal microscopy

Cells grown on glass cover slips were transfected and incubated with CHX (100 µg/ml) for 4 h prior to fixation. Cells were fixed in 4% paraformaldehyde and permeabilized with 10 mM phosphate-buffered saline, pH 7.4 containing 0.1% saponin as previously described [15]. After incubation with primary and fluorochrome-conjugated secondary antibodies, cover slips were sealed in mounting medium (DAKO, Glostrup, Denmark). Cells were analyzed using confocal laser scanning microscopy (Leica Model TCS-SL, Wetzlar, Germany) and images were merged using Adobe Photoshop software (Adobe Systems). In experiments using the polyclonal anti-FLAG antibody cells were fixed with methanol for 5 min at −20 °C followed by a 30-second incubation with acetone on ice. Cells were washed with phosphate-buffered saline and blocked with phosphate-buffered saline containing 1% BSA (PBS/BSA). Primary and secondary antibodies were diluted in PBS/BSA and the cover slips were processed as described above.

3. Results

3.1. The CLN7 membrane glycoprotein is proteolytically cleaved by cysteine proteases in acidic compartments

We previously showed that both CLN7 tagged N-terminally with green fluorescent protein (GFP-CLN7) and CLN7 tagged C-terminally with GFP (CLN7-GFP) are correctly sorted to lysosomes [15]. However, it was difficult to detect CLN7-GFP by Western blot analysis suggesting that the C-terminal domain of CLN7 is unstable. The intensity of the CLN7-GFP immunoreactive bands could be increased by the treatment of cells with a combination of cysteine and aspartic protease inhibitors suggesting proteolysis of the fusion protein in lysosomes.

To analyze proteolytic cleavage of CLN7 in detail, COS-7 cells were transiently transfected with a cDNA construct encoding CLN7 with an N-terminally appended triple FLAG tag (3xFLAG-CLN7, Fig. 1) allowing more-sensitive detection by immunoblotting (Fig. 2A). Western blot analyses of total cell extracts revealed a prominent immunoreactive band with apparent molecular masses ranging from 55 to 90 kDa (Fig. 2A, lane 2, open arrowhead) representing the heterogeneously *N*-glycosylated full-length CLN7 protein [15]. In addition, two specific immunoreactive bands at 57 and 53 kDa (arrows 1 and 2) and a 36 kDa immunoreactive band corresponding to an N-terminal fragment of CLN7 were observed (Fig. 2A, closed arrowhead). The 36 kDa band completely disappeared after raising the pH in endosomes and lysosomes with ammonium chloride (Fig. 2A, lane 3; also shown for HEK293 cells in Supplementary material, Fig. S1A, lane 2). This suggests

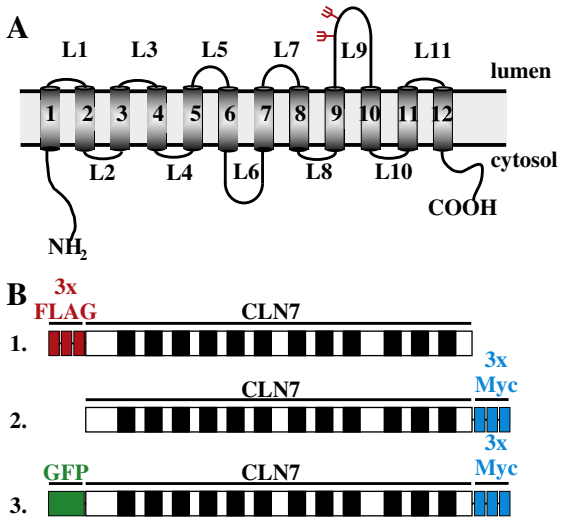

Fig. 1. Schematic representation of CLN7 membrane topology and used cDNA constructs. (A) Predicted topology model of the CLN7 membrane protein indicating orientation of the N- and C-terminal domains, loops L1-L11, the transmembrane domains 1–12, and the two used *N*-glycosylation sites at positions 371 and 376. (B) Schematic representation of the used CLN7 cDNA constructs with positions of the epitope tags.

that the 36 kDa CLN7 fragment is generated by proteolytic cleavage in acidic organelles. Furthermore, treatment of cells with the cysteine protease inhibitor E-64 [22] or the cysteine/serine protease inhibitor leupeptin [23] resulted in an increased intensity of the 55–90 kDa band accompanied by a strong reduction of the 36 kDa band (Fig. 2A, lanes 4 and 5; shown for HEK293 cells in Supplementary material, Fig. S1A, lanes 3 and 4). This indicated that cysteine proteases are involved in the cleavage of CLN7. In contrast, incubation of cells with the aspartic protease inhibitor pepstatin A did not alter the intensities of either the 55–90 kDa or the 36 kDa bands (Fig. 2A, lanes 6 and 7; shown for HEK293 cells in Supplementary material, Fig. S1A, lanes 5 and 6).

We have previously shown that CLN7 contains two used *N*-glycosylation sites in positions *N*371 and *N*376 [15]. To distinguish endoplasmic reticulum (ER) and *cis*-Golgi forms from *medial*- and post *medial*-Golgi forms of CLN7, COS-7 cells were transfected with 3xFLAG-CLN7 and total cell extracts were incubated in the absence or presence of endo H or PNGase F (Fig. 2B). After endo H treatment the electrophoretic mobilities of full-length CLN7 (55–90 kDa, open arrowhead) were unchanged indicating that both *N*-glycosylation sites contain complex-type oligosaccharides (Fig. 2B, lanes 2–4). The 57 kDa CLN7 form disappeared upon endo H treatment (Fig. 2B, lanes 2 and 3, arrow 1) accompanied by an increase in the intensity of the 53 kDa form (lanes 2 and 3, arrow 2) indicating that it represents the fraction of CLN7 containing high-mannose and hybrid *N*-linked oligosaccharides in the ER and *cis*-Golgi apparatus. As expected, PNGase F treatment resulted in the disappearance of the 55–90 kDa full-length CLN7 and the appearance of the 53 kDa form (Fig. 2B, lane 4). The results suggest that the heterogeneous band pattern of full-length CLN7 is due to the presence of complex *N*-linked oligosaccharide chains and confirms our earlier observations [15]. Furthermore, electrophoretic mobility of the 36 kDa N-terminal fragment (closed arrowhead) was not altered by PNGase F treatment. These results suggest that the 53 kDa band represents the non *N*-glycosylated CLN7 backbone protein and that the 36 kDa N-terminal CLN7 fragment contains no *N*-linked oligosaccharides. PNGase F treatment of cell extracts also resulted in the appearance of two additional bands with molecular masses of 47 and 38 kDa (Fig. 2B, lane 4, arrows 3 and 4). After endo H treatment no 38 kDa band could be detected indicating that this fragment is endo H-resistant and thus contains complex-type oligosaccharides (Fig. 2B, lanes 2 and 3).

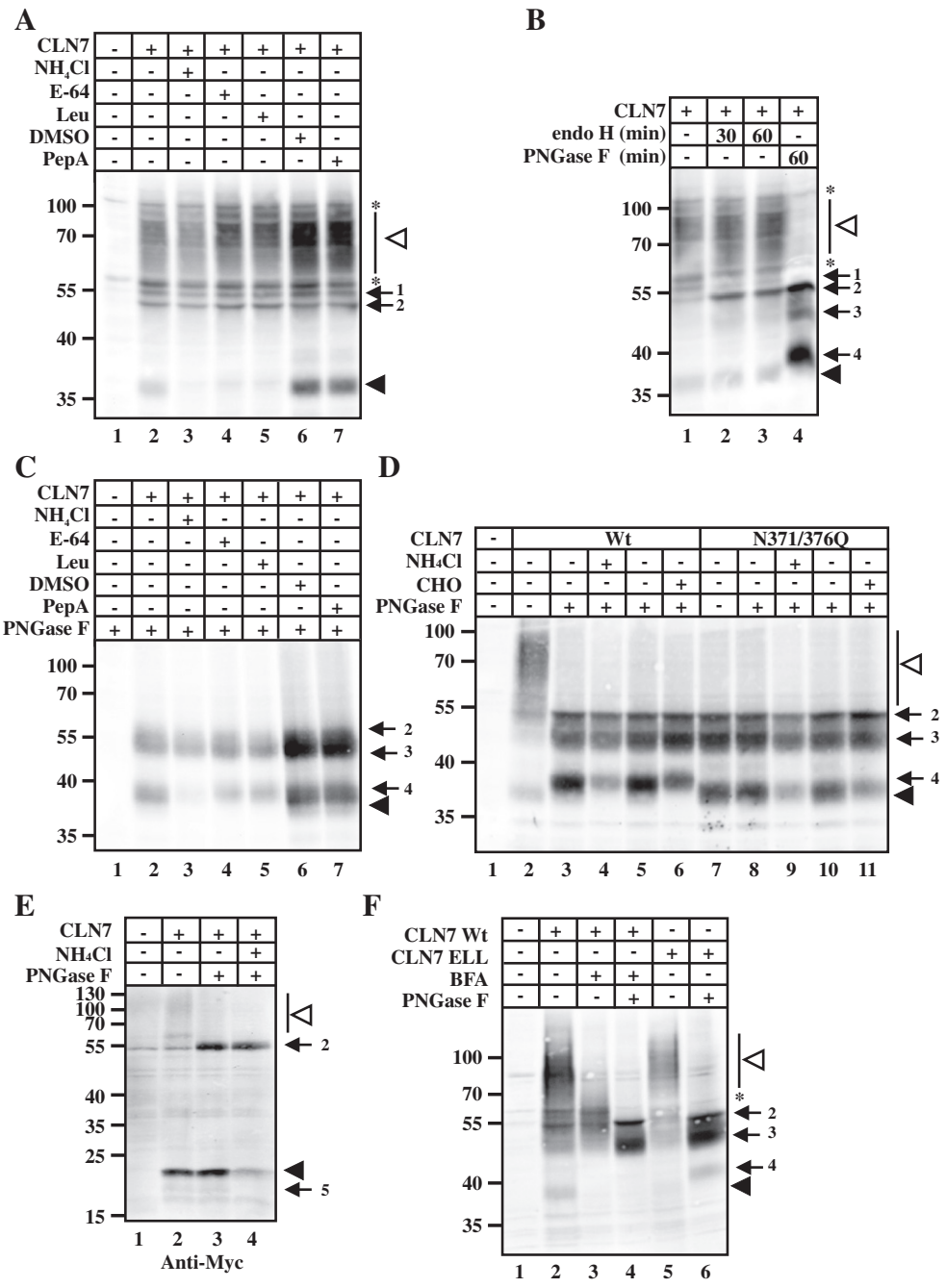

Fig. 2. The CLN7 membrane glycoprotein is proteolytically cleaved by cysteine proteases in acidic compartments. (A) COS-7 cells were mock-transfected (lane 1) or transfected with 3xFLAG-CLN7 cDNA and were incubated in the absence (-) or presence (+) of NH_4Cl (10 mM, lane 3), cysteine protease inhibitor E-64 (10 μg/ml, lane 4), cysteine/serine protease inhibitor leupeptin (Leu; 100 μM, lane 5), solvent control (DMSO, lane 6), or aspartic protease inhibitor pepstatin A (Pep A, 100 μM, lane 7) for 24 h. Total cell extracts (50 μg) were separated by SDS-PAGE and analyzed by FLAG immunoblotting. (B) Total cell extracts (50 μg) from COS-7 cells expressing 3xFLAG-CLN7 were incubated in the absence (-; lane 1) or presence of endo H (lanes 2 and 3) or peptide N-glycosidase F (PNGase F; lane 4) for the indicated time periods and analyzed by FLAG immunoblotting. (C) COS-7 cells were transfected and treated with inhibitors as described for Fig. 2A and total cell extracts (50 μg) were treated with PNGase F and analyzed by FLAG Western blotting. (D) COS-7 cells were mock-transfected (lane 1), transfected with wild-type 3xFLAG-CLN7 or 3xFLAG-CLN7 N371/376Q cDNA and treated with NH_4Cl (10 mM; lanes 4 and 9) or the cathepsin L inhibitor Z-FY-CHO (CHO, 10 μM, lanes 6 and 11). Subsequently total cell extracts (50 μg) were incubated with PNGase F and analyzed by FLAG immunoblotting. (E) COS-7 cells were mock-transfected (lane 1) or transfected with CLN7-3xMyc (lanes 2–4) and were incubated in the absence (-) or presence (+) of NH_4Cl (10 mM, lane 4). Total cell extracts (50 μg) were incubated with PNGase F (lanes 3 and 4) and analyzed by Myc immunoblotting. Positions of the full-length CLN7 (open arrowhead), the 20 kDa C-terminal fragment (closed arrowhead) and the 18 kDa C-terminal fragment (arrow 5) are indicated. (F) COS-7 cells were mock-transfected (lane 1) or transfected with wild-type 3xFLAG-CLN7 (Wt) or 3xFLAG-CLN7 E9A L13A L14A (ELL) and incubated in the absence (-, lanes 1–2 and 5–6) or presence (+; lanes 3 and 4) of brefeldin A (BFA). Cells were harvested and total cell extracts (50 μg) were incubated with control buffer (-; lanes 1–3 and lane 5) or PNGase F (+; lanes 4 and 6) and analyzed by FLAG immunoblotting. Panels A, B, C, D and F: The positions of full-length CLN7 (open arrowhead), *N*-glycosylated ER/*cis*-Golgi-localized (arrow 1), non *N*-glycosylated full-length CLN7 (arrow 2), the 47 kDa form (arrow 3), the 38 kDa fragment (arrow 4) and the 36 kDa fragment (closed arrowhead) are indicated. Non-specific bands are indicated by asterisks.

We next asked whether the 38 kDa and 47 kDa bands also result from the cleavage of CLN7 by lysosomal cysteine/serine proteases. In extracts of COS-7 cells incubated in the presence of ammonium chloride and treated with PNGase F prior to immunoblotting the intensity of the 38 kDa band decreased compared to non-treated cells (Fig. 2C, lane 3). This suggests that the 38 kDa CLN7 fragment is also generated by proteolytic cleavage. To a lesser extent, treatment of cells with the inhibitors E-64 or leupeptin also resulted in a reduction of the 38 kDa band

(Fig. 2C, lanes 4 and 5). This indicated that cysteine proteases are involved in two cleavage events in CLN7: one that results in a non *N*-glycosylated 36 kDa fragment and one that results in an *N*-glycosylated fragment with an apparent molecular mass of 38 kDa after deglycosylation with PNGase F. Incubation of cells with the aspartic protease inhibitor pepstatin A did not alter the intensity of the 38 kDa band (Fig. 2C, lanes 6 and 7). Although the 47 kDa band is difficult to distinguish from the 53 kDa band in Fig. 2C, its intensity does not change upon treatment with ammonium chloride, E-64, leupeptin or pepstatin A. This suggests that the 47 kDa band is the product of a non-lysosomal cleavage event. Alternatively, it may represent full-length non *N*-glycosylated CLN7 and the 53 kDa form may be the result of an additional post-translational modification. In an additional experiment, COS-7 cells were transfected with 3xFLAG-CLN7 cDNA and treated with NH_4Cl or Z-FY-CHO, which inhibits the cysteine protease cathepsin L [24]. The 36 kDa CLN7 fragment (closed arrowhead) disappeared completely after treatment with either NH_4Cl or Z-FY-CHO. Treatment of cells with NH_4Cl resulted in a 40% decrease in the amount of 38 kDa fragment (Fig. 2D, lane 4), while treatment with Z-FY-CHO resulted in a 33% decrease (Fig. 2D, lane 6). Overexpression of the *N*-glycosylation-defective 3xFLAG-CLN7 N371/376Q [15] resulted in immunoreactive bands at 36, 47 and 53 kDa, but not at 38 kDa (Fig. 2D, lanes 8–11). The 36 kDa band is stronger in 3xFLAG-CLN7 N371/376Q than in 3xFLAG-CLN7 wild-type and is more sensitive to NH_4Cl than to Z-FY-CHO. Quantitation of proteolytic cleavage showed that the 36 kDa CLN7 fragment comprises 9.5% ($\pm$4.3%, n = 6) of cellular CLN7, while the 38 kDa CLN7 fragment comprises 47.3% ($\pm$7.1%, n = 6) of cellular CLN7. Therefore, 56.8% of cellular CLN7 polypeptide is proteolytically cleaved. After the removal of the *N*-glycosylation sites the 38 kDa fragment is no longer present and the 36 kDa fragment comprises 33.9% ($\pm$2.2%, n = 6) of cellular CLN7, suggesting that *N*-glycosylation inhibits the cleavage event that generates the 36 kDa fragment. These results indicate that the 36 kDa and 38 kDa fragments are proteolytic cleavage products. CLN7 is proteolytically cleaved twice, once proximal to the *N*-glycosylation sites in lumenal loop L9 and once distal to these sites. No conclusions could be drawn about the origin of the 47 kDa fragment.

To analyze the identity of the C-terminal cleavage fragment, COS-7 cells overexpressing CLN7 with a C-terminal triple Myc tag (CLN7-3xMyc) were also analyzed (Fig. 2E). Cells expressing CLN7-3xMyc were incubated in the absence or presence of NH_4Cl and total cell extracts were analyzed by FLAG immunoblotting. Full-length CLN7-3xMyc and its C-terminal fragment were detected as bands with apparent molecular masses of 70–130 kDa (Fig. 2E, open arrowhead) and 20 kDa (Fig. 2E, closed arrowhead), respectively. After PNGase F treatment the molecular mass of full-length CLN7 shifted to 55 kDa (lanes 3 and 4, arrow 2) but the 20 kDa C-terminal fragment was insensitive to PNGase F indicating that CLN7 is first cleaved distal to the two *N*-glycosylation sites resulting in a non *N*-glycosylated C-terminal CLN7 fragment (Fig. 2E, lane 3). Furthermore, cleavage of CLN7-3xMyc could be inhibited by incubation of the cells in the presence of NH_4Cl indicating the cleavage in acidic compartments (Fig. 2E, lane 4). A small amount of a second fragment of approximately 18 kDa was detected, which was also sensitive to NH_4Cl treatment (Fig. 2E, arrow 5). Quantitation of the immunoreactive band intensities showed that the 20 kDa CLN7 fragment comprises 27.4% ($\pm$10.4%, n = 10) of cellular CLN7. The second, consecutive cleavage event, which occurs proximal to the two *N*-glycosylation sites, can only be detected with N-terminally tagged CLN7 constructs.

To analyze whether cleavage of CLN7 occurs in the endoplasmic reticulum (ER), COS-7 cells expressing 3xFLAG-CLN7 were incubated in the presence of brefeldin A (BFA) to inhibit anterograde transport from the ER to the Golgi apparatus [25]. Treatment of the cells with BFA resulted in complete disappearance of the 36 kDa immunoreactive band (Fig. 2F, lane 3, closed arrowhead) as well as an overall reduced signal for CLN7, possibly reflecting inhibition of protein translation due to accumulation of proteins in the ER. As expected, the 57 kDa CLN7 form, representing CLN7 containing high-mannose and hybrid *N*-linked oligosaccharides in the ER and *cis*-Golgi apparatus (Fig. 2B), disappeared upon PNGase F treatment accompanied by an increase in the intensity of the non *N*-glycosylated CLN7 with an apparent molecular mass of 53 kDa (Fig. 2F, lane 4). The additional 47 kDa band could also be detected after treatment of cells with BFA and incubation of cell extracts with PNGase F (Fig. 2F, lane 4), suggesting that this form of CLN7 is generated in the ER. However, the 38 kDa band is not visible in these cells, indicating that this form of CLN7 is generated post-ER. Proteolytic cleavage was also analyzed in COS-7 cells transfected with mutant 3xFLAG-CLN7 E9A L13A L14A cDNA, which is partially missorted to the plasma membrane [15]. In these cells the intensity of the 36 kDa immunoreactive band was strongly decreased (Fig. 2F, lane 5). PNGase F treatment resulted in the appearance of the 47 and 38 kDa bands, but the intensity of the 38 kDa band was much weaker than in cells transfected with wild-type 3xFLAG-CLN7 (compare Fig. 2F, lane 6 with Fig. 2D, lane 3), suggesting that some 3xFLAG-CLN7 E9A L13A L14A is correctly targeted to lysosomes. In summary, after deglycosylation, four forms of CLN7 with molecular masses of 36, 38, 47 and 53 kDa were detected. The 36 kDa and 38 kDa forms are products of proteolytic cleavage in acidic organelles, while the 47 kDa and 53 kDa forms are already present in the ER.

To determine the subcellular localization of the N- and C-terminal domains, a CLN7 construct with GFP fused to its N terminus and a triple Myc epitope tag fused to its C terminus (GFP-CLN7-3xMyc) was transfected into COS-7 cells. Localization of the N- and C-terminal domains was detected by GFP fluorescence and Myc- immunostaining, respectively. Both the N- and C-terminal domains of CLN7 co-localized in LAMP-1 positive compartments (Fig. 3A, panels c and d, g and h). In combination with the above findings, this suggests that the GFP-CLN7-3xMyc protein is still intact when it reaches the lysosomes where it is proteolytically cleaved.

To determine if the N- and C-terminal CLN7 fragments interact with the parental molecule, co-immunoprecipitations were performed. HEK293 cells were co-transfected with GFP-CLN7 and 3xFLAG-CLN7 or with GFP-CLN7 and CLN7-3xMyc and lysates were submitted to GFP immunoprecipitation using GFP-TRAP® (Fig. 3B). Both full-length 3xFLAG-CLN7 and CLN7-3xMyc (Fig. 3B, upper panels, lanes 2–4 and 6–8), as well as the N-terminal 3xFLAG-CLN7 fragment (Fig. 3B, upper panel, lanes 2–4) co-precipitated with GFP-CLN7, suggesting an interaction between full-length CLN7 polypeptides and full-length CLN7 and the N-terminal fragment. A weak binding of full-length CLN7 to the 18 kDa and 20 kDa C-terminal fragments was observed, which became detectable after longer exposure times (Fig. 3B, upper and middle panels, lanes 6–8).

3.2. Proteolytic cleavage of CLN7 is mediated by cathepsin L

COS-7 cells overexpressing 3xFLAG-CLN7 were treated with increasing concentrations (1–50 μM) of the membrane permeable Ctsl inhibitors SID26681509 [26] and Z-FY-CHO [27]. Analysis of total cell extracts by FLAG immunoblotting revealed that SID26681509 partially inhibited cleavage of CLN7 in a dosage-dependent manner as shown by the decreased intensity of the 36 kDa fragment (Fig. 4A, lanes 3–6, closed arrowhead) whereas Z-FY-CHO almost completely inhibited cleavage at concentrations of 1 μM or higher (Fig. 4A, lanes 7–10). The amount of full-length CLN7 also decreased when cells are treated with SID26681509 or Z-FY-CHO but to a lesser extent than the 36 kDa fragment. This becomes clear when quantitating the amount of the 36 kDa cleavage fragment as a percentage of total CLN7 (Fig. 4A, right panel). The effect of Ctsl inhibitors on the generation of the 38 kDa fragment was studied by treating cells with SID26681509 and Z-FY-CHO and incubating the cell lysates with PNGase F prior to FLAG immunoblotting (Fig. 4B). Treatment of cells with SID26681509 did not significantly decrease the amount of the 38 kDa fragment, whereas Z-FY-CHO treatment resulted in a reduced intensity of the 38 kDa band at

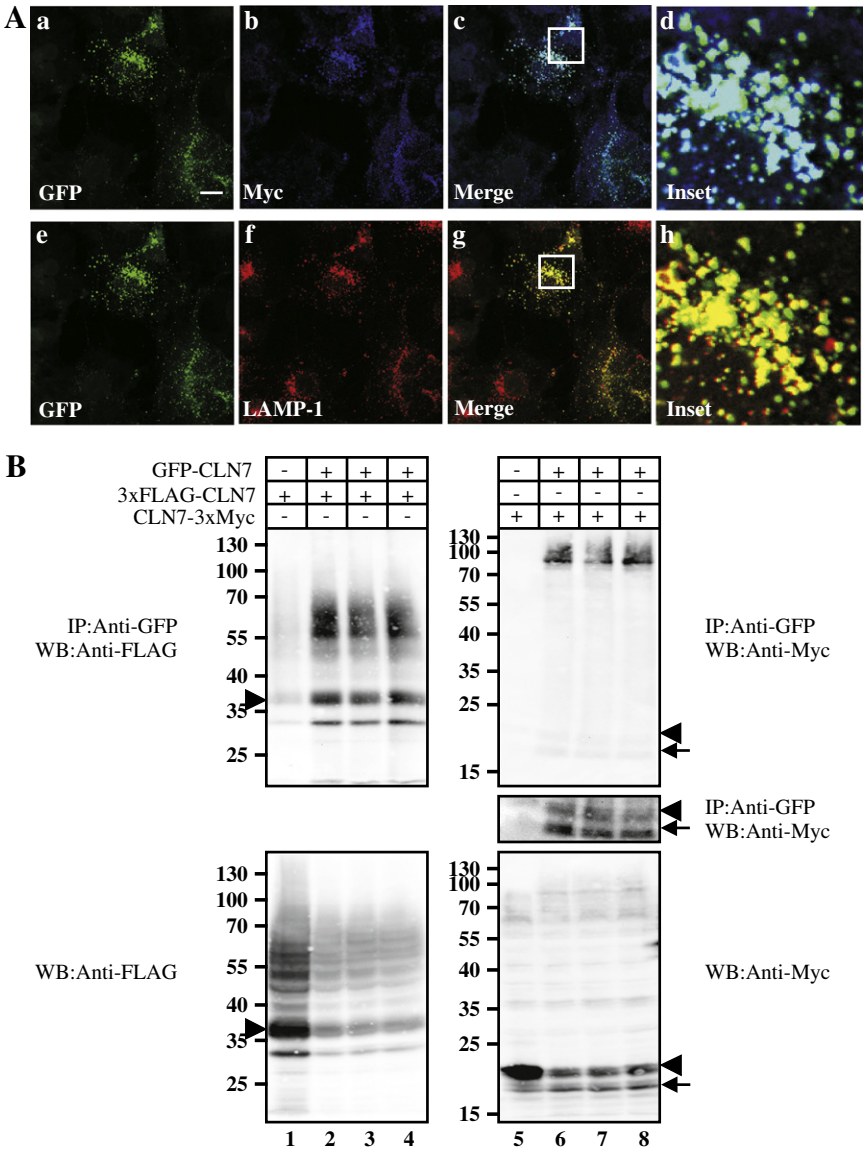

Fig. 3. Lysosomal localization and interactions of full-length CLN7. (A) COS-7 cells were transfected with GFP-CLN7-3xMyc cDNA. Prior to fixation, cells were treated with CHX (100 μg/ml) for 4 h and then incubated with antibodies against c-Myc (b, purple) and the lysosomal marker protein LAMP-1 (f, red). CLN7 fragments were either visualized by GFP-fluorescence (a and e, green) or by anti-rabbit antibodies coupled to Cy5 (b, purple). LAMP-1 was detected by anti-mouse secondary antibodies coupled to AlexaFluor 546 (f, red). Merged images (c, d, g and h) indicate co-localization. Insets d and h represent 6.5-fold higher magnification images of the regions marked by the white squares. Scale bar, 10 μm. (B) HEK293 cells were transfected with 3xFLAG-CLN7 and empty vector (lane 1), GFP-CLN7 and 3xFLAG-CLN7 (lanes 2–4), CLN7-3xMyc and empty vector (lane 5) or GFP-CLN7 and CLN7-3xMyc (lanes 6–8). Lysates were submitted to GFP immunoprecipitation followed by SDS-PAGE of eluates and immunostaining with anti-FLAG (10% acrylamide, left panels, representative of 3 experiments) or anti-Myc (12.5% acrylamide, right panels, representative of 4 experiments). C-terminal fragments were visualized by longer exposure times (middle right panel). Lysates (20% of total) were analyzed by anti-FLAG immunostaining (bottom, left panel) or anti-Myc immunostaining (bottom, right panel). The N-terminal and C-terminal fragments are indicated. Lanes 2 through 4 and lanes 6 through 8 are samples derived from independent transfections. IP, immunoprecipitation; WB, Western blot.

concentrations of 1 μM or higher (Fig. 4B, right panel). The 47 kDa band was not affected by treatment with SID26681509 or Z-FY-CHO (Fig. 4B).

To verify Ctsl-mediated cleavage of CLN7 by an independent approach, CLN7 was expressed in both wild-type (*Ctsl*$^{(+/+)}$) and *Ctsl*-deficient mouse embryonic fibroblasts (*Ctsl*$^{(-/-)}$ MEF). In extracts from transfected wild-type MEF both the 55–90 kDa band (open arrowhead) and the 36 kDa CLN7 fragment (closed arrowhead) could be detected by FLAG immunoblotting (Fig. 5A, lanes 1–3). In contrast, in *Ctsl*$^{(-/-)}$ MEF only the 55–90 kDa full-length CLN7 but not the 36 kDa fragment was observed, indicating that the absence of Ctsl prevents proteolytic cleavage of CLN7 (Fig. 5A, lanes 4–6). Cleavage of CLN7 expressed in cathepsin B-deficient (*Ctsb*$^{(-/-)}$) MEF was not affected (not shown). Cell lysates were also treated with PNGase F but, interestingly, the 38 kDa fragment could be detected both in wild-type and in *Ctsl*$^{(-/-)}$ MEF (Fig. 5B), suggesting that Ctsl is not required for the cleavage.

Next, we determined whether expression of Ctsl could rescue the proteolytic cleavage of CLN7 in *Ctsl*$^{(-/-)}$ MEF. *Ctsl*$^{(-/-)}$ MEF were either mock-transfected or co-transfected with 3xFLAG-CLN7 and murine Ctsl or 3xFLAG-CLN7 and murine Ctsb cDNA. Co-expression of Ctsl could rescue proteolytic cleavage of CLN7 in *Ctsl*$^{(-/-)}$ MEF (Fig. 5C, lanes 5 and 6), whereas co-expression of Ctsb cDNA had a smaller effect (Fig. 5C, lanes 3 and 4). Therefore, we conclude that the lysosomal cysteine protease Ctsl is required for generation of the 36 kDa fragment, but not for the formation of the 38 kDa fragment. No effect of Ctsl overexpression on the amount of the 38 kDa fragment was observed in *Ctsl*$^{(-/-)}$ MEF (Fig. 5D).

3.3. Cleavage of CLN7 occurs in luminal loop L9

Based on the apparent molecular masses and *N*-glycosylation pattern of the N-terminal cleavage products, we hypothesized that

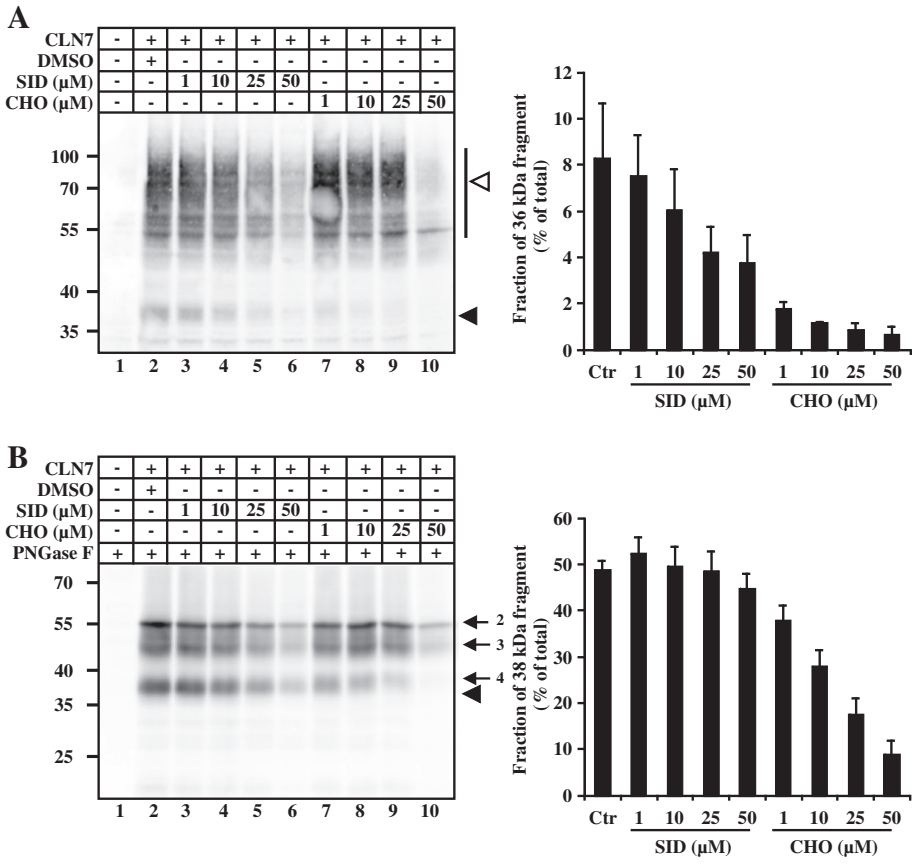

Fig. 4. Proteolytic cleavage of CLN7 is mediated by cathepsin L (Ctsl). (A) Dosage-dependent inhibition of proteolytic cleavage by Ctsl inhibitors. COS-7 cells were mock-transfected (lane 1) or transfected with 3xFLAG-CLN7 and incubated in the absence (DMSO, lane 2) or presence of increasing concentrations of the Ctsl inhibitors SID26681509 (SID, lanes 3–6) and Z-FY-CHO (CHO, lanes 7–10). Total cell extracts (50 μg) were separated by SDS-PAGE and analyzed by FLAG immunoblotting. Intensities of immunoreactive bands corresponding to the full-length CLN7 (open arrowhead) and the 36 kDa fragment (closed arrowhead) were quantified densitometrically and the mean fraction ± standard deviation of the N-terminal fragment is shown in a bar diagram (right panel). (B) Cells were transfected and treated with inhibitors as described for Fig. 4A and total cell extracts (50 μg) were treated with PNGase F. Intensities of immunoreactive bands corresponding to the full-length CLN7 (arrows 2 and 3) and the 38 kDa fragment (arrow 4) were quantified densitometrically and the mean fraction ± standard deviation of the N-terminal fragment is shown in a bar diagram (right panel).

cleavage occurs in lumenal loop L9 of CLN7 (Fig. 1). We previously observed that the apparent molecular mass of non *N*-glycosylated CLN7 is smaller than predicted based on the amino acid composition [15]. Therefore, we generated C-terminal truncation mutants to further confine the predicted cleavage site. Premature stop codons were inserted proximal to the first *N*-glycosylated asparagine residue, N371 (CLN7 H370X), at the end of loop L9 (CLN7 H415X) and at the end of loop L11 (CLN7 R482X) based on the predicted topology of CLN7 and the identified *N*-glycosylation sites [9,15] (Fig. 6A). COS-7 cells were transiently transfected with wild-type and truncated CLN7 cDNA constructs and total cell extracts were incubated in the absence or presence of PNGase F followed by FLAG immunoblotting (Fig. 6B). The electrophoretic mobilities of the 36 kDa N-terminal CLN7 cleavage product and the truncated CLN7 H370X polypeptide were comparable (Fig. 6B, lanes 3–5). As expected the electrophoretic mobility of the CLN7 H370X polypeptide was unchanged after PNGase F treatment indicating the absence of *N*-linked oligosaccharides (Fig. 6B, lane 5). In extracts from cells expressing CLN7 H415X or CLN7 R482X immunoreactive bands with slower electrophoretic mobility corresponding to molecular masses of 51 kDa and 53 kDa were detected (Fig. 6B, lanes 6 and 8). After PNGase F treatment of cell homogenates molecular masses of CLN7 H415X and R482X polypeptides shifted to 42 kDa and 40 kDa, respectively, indicating the presence of *N*-linked oligosaccharides (Fig. 6B, lanes 7 and 9). Thus, the 38 kDa CLN7 fragment observed after deglycosylation with PNGase F is likely generated by proteolytic cleavage between residues 370 and 415 in loop L9 (Fig. 2B). These results suggest that both the 36 kDa and the 38 kDa CLN7 fragments are generated by proteolytic cleavage in lumenal loop L9 of CLN7. The apparent molecular masses of the full-length and truncated CLN7 polypeptides are shown in the diagram in Fig. 6A. Both 3xFLAG-CLN7 H370X and 3xFLAG-CLN7 H415X did not co-localize with the lysosomal marker protein cathepsin D suggesting their retention in the endoplasmic reticulum (Supplementary material, Fig. S2). Hence no N-terminal cleavage fragment was observed for CLN7 H415X in Western blot analyses (Fig. 6B). In contrast, CLN7 R482X was co-localized with cathepsin D indicating its transport to lysosomes. (Supplementary material, Fig. S2). However no N-terminal cleavage fragment was observed (Fig. 6B).

3.4. The CLN7 precursor is gradually cleaved

To examine the half-life of CLN7 and the kinetics of proteolytic cleavage, a CHX pulse-chase experiment was performed in cells expressing 3xFLAG-CLN7 or the *N*-glycosylation mutant 3xFLAG-CLN7 N371/376Q (Fig. 7A). 24 h after the start of transfection, cells were treated with CHX to inhibit new protein biosynthesis. Cells were harvested at different time points and total cell extracts were analyzed by FLAG immunoblotting. The intensities of the 55–90 kDa CLN7 bands decreased in the presence of CHX during the first 24-hour interval, whereas the intensities of the 36 kDa CLN7 fragment increased (Fig. 7A, lanes 2–4). An additional 33 kDa immunoreactive band was detected in cells expressing wild-type (Fig. 7A, lanes 2–5) and non *N*-glycosylated CLN7 N371/376Q (Fig. 7A, lanes 6–9). However, after

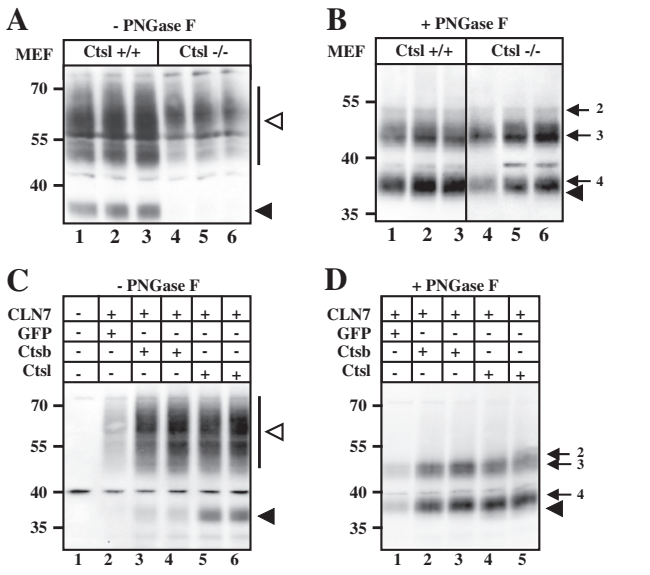

Fig. 5. Proteolytic cleavage of CLN7 in Ctsl-deficient mouse embryonic fibroblasts (MEF). (A) Wild-type (*Ctsl*$^{(+/+)}$) and Ctsl-deficient (*Ctsl*$^{(-/-)}$) MEF were transfected with 3xFLAG-CLN7 and total extracts (50 μg) analyzed by FLAG immunoblotting. (B) Wild-type (*Ctsl*$^{(+/+)}$) and *Ctsl*$^{(-/-)}$ MEF were transfected with 3xFLAG-CLN7 and total cell extracts (50 μg) were treated with PNGase F. Extracts were separated by SDS-PAGE and analyzed by FLAG immunoblotting. Exposure time of the blot derived from extracts of *Ctsl*$^{(-/-)}$ MEF was two-fold longer. (C) Proteolytic cleavage generating the 36 kDa fragment can be rescued by overexpression of Ctsl. *Ctsl*$^{(-/-)}$ MEF were mock-transfected (lane 1) or co-transfected with 3xFLAG-CLN7 and GFP (lane 2), Ctsb (lanes 3 and 4) or Ctsl cDNAs (lanes 5 and 6). Total cell extracts (50 μg) were separated by SDS-PAGE and analyzed by FLAG immunoblotting. (D) Cells were transfected as described for Fig. 5C and total cell extracts (50 μg) were treated with PNGase F. Positions of full-length CLN7 (open arrowhead) and its N-terminal fragment (closed arrowhead) are indicated in panels A and C; positions of non *N*-glycosylated full-length CLN7 (arrow 2), the 47 kDa form (arrow 3), the 38 kDa fragment (arrow 4) and the 36 kDa fragment (closed arrowhead) are indicated in panels B and D.

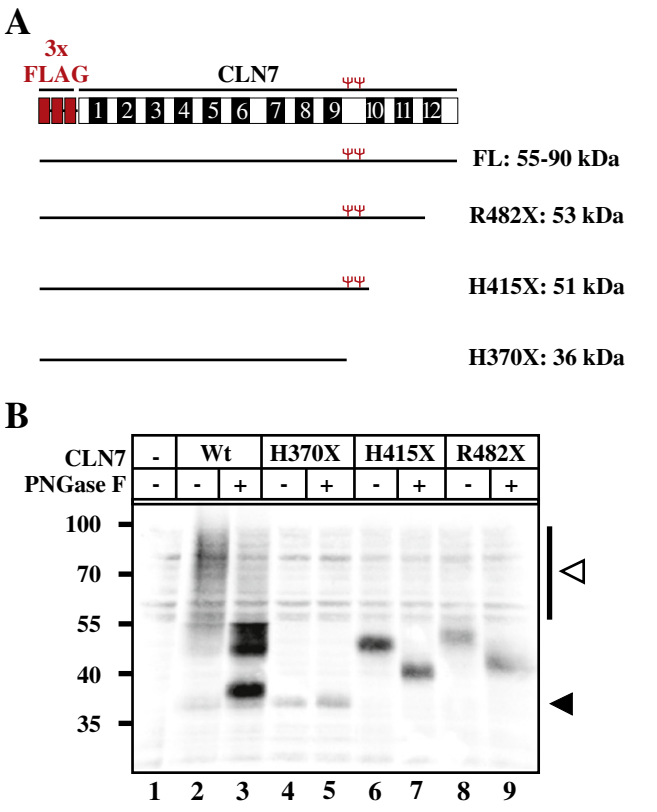

Fig. 6. CLN7 is cleaved in lumenal loop L9. (A) Schematic representation of wild-type and truncated CLN7 polypeptides and their apparent molecular masses. Transmembrane domains are numbered as black boxes and the positions of used *N*-glycosylation sites N371 and N376 are shown. (B) COS-7 cells were mock-transfected (lane 1), transfected with wild-type 3xFLAG-CLN7 (lanes 2 and 3; Wt) or mutant 3xFLAG-CLN7 with C-terminal deletions resulting in truncations prior to the first *N*-glycosylation site (lanes 4 and 5; p.H370X), at the end of lumenal loop L 9 (lanes 6 and 7; p.H415X) or at the end of lumenal loop L11 (lanes 8 and 9; p.R482X). Aliquots of total cell extracts were incubated in the absence (-) or presence (+) of PNGase F. Cell extracts (50 μg) were separated by SDS-PAGE and analyzed by FLAG immunoblotting. Positions of molecular mass markers in kDa, full-length CLN7 (open arrowhead) and its N-terminal fragment (closed arrowhead) are indicated.

48 h, the intensities of the 55–90 kDa, the 36 kDa and the 33 kDa bands decreased (Fig. 7A, lane 5). Similar results were obtained for the *N*-glycosylation-defective 3xFLAG-CLN7 N371/376Q mutant, although the ratio of N-terminal fragment to full-length CLN7 was increased and cleavage appeared to peak earlier, after 8 h of CHX treatment (Fig. 7A, lanes 6–9). The cDNA construct 3xFLAG-mucolipin-1 (3xFLAG-ML1) was used as a control coding for a polytopic *N*-glycosylated membrane protein which is cleaved in lysosomes (Fig. 7A, lanes 10–12). During the entire 48-hour CHX-chase the intensity of the full-length ~70 kDa 3xFLAG-ML1 immunoreactive band decreased whereas the amount of the N-terminal ~40 kDa cleavage product increased (Fig. 7A, lanes 10–12). To study the kinetics of proteolysis and the stability of the 38 kDa cleavage product, the CHX pulse-chase experiment was repeated and total cell extracts were incubated in the absence or presence of PNGase F prior to FLAG Western blotting (Fig. 7B). Similar to Fig. 7A, the intensities of the 55–90 kDa CLN7 bands initially decreased in the presence of CHX, whereas the intensities of the 36 kDa CLN7 fragment initially increased. The intensity of the 38 kDa band observed for 3xFLAG-CLN7 after PNGase F treatment was most intense after 8 h of CHX treatment (Fig. 7B, lanes 6–10).

3.5. CLN7 mutations p.T294K and p.P412L alter proteolytic cleavage

To date 31 different mutations have been identified in the *CLN7/MFSD8* gene in patients with CLN7 disease [9–13]. To investigate the impact of mutations on expression and proteolytic cleavage, mutant CLN7 cDNAs were transiently transfected into COS-7 cells and total cell extracts were analyzed by Western blotting. Only mutations in the C-terminal half of the CLN7 protein were selected for these studies, which are located in the vicinity of the potential cleavage site in loop L9 (Fig. 8A). The same immunoreactive bands were observed in extracts from COS-7 cells expressing wild-type and mutant 3xFLAG-CLN7 (Fig. 8B) suggesting correct folding and lysosomal targeting of mutant CLN7 proteins followed by cleavage in lysosomes. However, in extracts from cells expressing mutant CLN7 p.T294K the intensity of a 33 kDa immunoreactive band was increased (Fig. 8B, lane 3). In addition, the intensity of the 36 kDa fragment in COS-7 cells expressing CLN7 p.P412L was enhanced in comparison with wild-type CLN7 (Fig. 8B, lane 6). When cells overexpressing mutant CLN7 p.P412L and p.T294K were treated with the Ctsl inhibitor Z-FY-CHO the intensities of the 55–90 kDa immunoreactive band were increased whereas the intensities of the 36 kDa and 33 kDa fragments were strongly reduced (Supplementary material, Fig. S1B), indicating that cleavage of mutant CLN7 polypeptides is also mediated by Ctsl.

The p.G310D, p.D368H, p.G429D and p.R465W mutations did not significantly affect proteolytic cleavage of CLN7 (Fig. 8B, lanes 4, 5, 7 and 8). These results suggest that the p.T294K and p.P412L mutations in CLN7 alter the conformation of lumenal loops L7 and L9, respectively, resulting in increased cleavage. Both wild-type and mutant 3xFLAG-CLN7-polypeptides were mainly localized in lysosomal compartments as shown by co-distribution with the lysosomal membrane protein LAMP-1 (Fig. 8C). In agreement with these findings, wild-type and mutant CLN7-3xMyc polypeptides co-

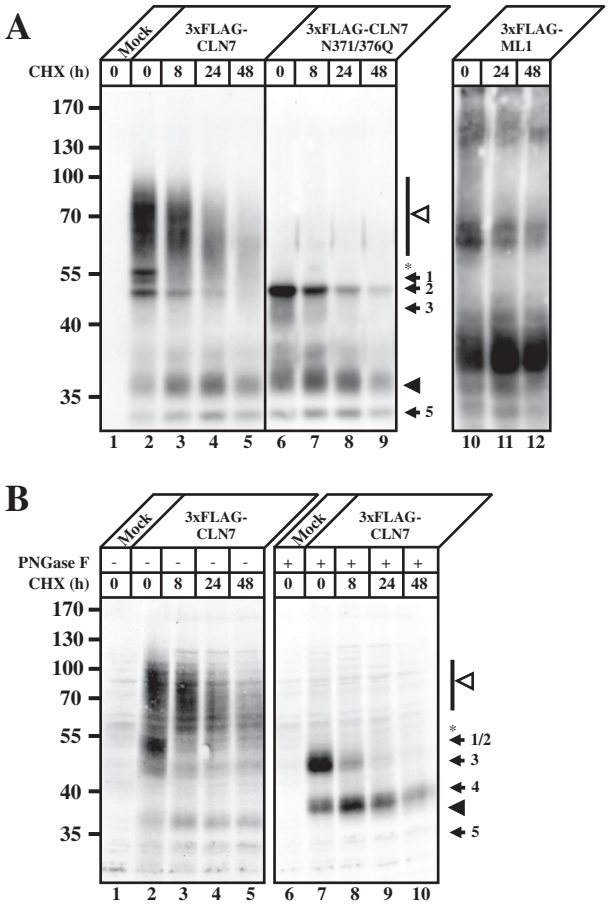

Fig. 7. The CLN7 precursor is gradually cleaved. (A) COS-7 cells were mock-transfected (lane 1) or transfected with 3xFLAG-CLN7 (lanes 2–5), 3xFLAG-CLN7 N371/376Q (lanes 6–9) or 3xFLAG-mucolipin-1 cDNAs (3xFLAG-ML1, lanes 10–12). At 24 h after transfection, cells were either harvested or incubated in the presence of 100 μg/ml cycloheximide (CHX) for the indicated time intervals. Total cell extracts (25 μg) were separated by SDS-PAGE and analyzed by FLAG immunoblotting. (B) COS-7 cells were mock-transfected (lanes 1 and 6) or transfected with 3xFLAG-CLN7 cDNA (lanes 2–5 and lanes 7–10). Total cell extracts (50 μg) were incubated in the absence (-; lanes 1–5) or presence of PNGase F (+; lanes 6–10) for 1 h and analyzed by Western blotting using anti-FLAG. Positions of full-length CLN7 (open arrowhead), *N*-glycosylated ER/*cis*-Golgi-localized (arrow 1), non *N*-glycosylated CLN7 (arrow 2), the 47 kDa fragment (arrow 3), 38 kDa fragment (arrow 4), the N-terminal 36 kDa fragment (closed arrowhead) and an additional band at 33 kDa (arrow 5) are indicated.

localized with the lysosomal marker protein LAMP-1, indicating that lysosomal localization was independent of the 3xFLAG epitope tag (Supplementary material, Fig. S3).

4. Discussion

In the present study we demonstrate that full-length CLN7 is proteolytically cleaved twice. Expression analyses in the presence of pharmacological inhibitors of lysosomal acidification or of lysosomal proteases showed that cleavage of CLN7 occurs in acidic compartments and is mediated by lysosomal cysteine proteases. Furthermore, we demonstrated that correct lysosomal targeting of CLN7 is required for proteolytic cleavage. Retention of CLN7 in the endoplasmic reticulum by incubation of the cells with BFA resulted in complete inhibition of proteolytic cleavage, while mistargeting of CLN7 to the plasma membrane by mutation of its N-terminal dileucine-based lysosomal sorting motif resulted in reduction of proteolytic cleavage. A comparison of the apparent molecular masses of the N-terminal CLN7 fragment with truncated CLN7 polypeptides suggested that proteolytic cleavage occurs in lumenal loop L9. Lumenal loop L9 of the human CLN7 membrane protein is *N*-glycosylated at positions N371 and N376 [15] and is the largest lumenal loop within CLN7, encompassing 58 amino acids, which may favor steric access for proteolytic enzymes in the lysosomal lumen. It would be of interest to know how the uncleaved fraction of CLN7 polypeptides is protected from proteolytic cleavage. A possible explanation is that *N*-glycosylation of lumenal loop L9 of CLN7 limits the rate of proteolysis as it does for LAMP-1 and LAMP-2 [28]. Indeed we found increased cleavage generating the 36 kDa fragment in non *N*-glycosylated CLN7. Surprisingly, the N-terminal 38 kDa fragment comprises 47.5% of total cellular CLN7, while the C-terminal 20 kDa fragment only comprises 27.4% of cellular CLN7. This may be due to lower stability of the C-terminal fragment.

It is expected that inhibition of lysosomal acidification by ammonium chloride would reduce proteolytic cleavage leading to an increase of full-length CLN7. However, we observed no increased levels of full-length CLN7 (Fig. 2A, lane 3; Fig. 2D, lanes 4 and 9; Fig. 2E, lane 4; Fig. S1A, lane 2), suggesting decreased protein expression in the presence of ammonium chloride. Interestingly, Savalas and co-workers also observed inhibition of proteolytic cleavage for the lysosomal MFS transporter DIRC2 by ammonium chloride and no concomitant increase in the amount of full-length DIRC2 [19]. In contrast, treatment of the cells with cysteine protease inhibitor E-64 or the cysteine/serine protease inhibitor leupeptin resulted in an inhibition of proteolytic cleavage accompanied by an increased amount of full-length CLN7.

After the lysosomal transporter DIRC2, CLN7 is the second member of the MFS that is found to be proteolytically cleaved [19,29] and the first example of a disease-associated lysosomal membrane protein that is processed by Ctsl. Furthermore, CLN7 is the first member of the MFS that appears to interact non-covalently with other CLN7 polypeptides [17]. We observed a high-affinity interaction between the N-terminal fragment and full-length CLN7, but a low-affinity interaction between the C-terminal fragment and full-length CLN7.

The cycloheximide pulse-chase experiments revealed that CLN7 is gradually cleaved and that only small amounts of full-length CLN7 remain after chase periods of 24 and 48 h. In addition, the presence of distinct 38 kDa, 36 kDa and 33 kDa CLN7 fragments, which have considerable stability in lysosomes suggests that they do not represent degradation intermediates. However, the significance of proteolytic cleavage for the biological functions of CLN7 is presently unclear as the substrates and precise functions of CLN7 are unknown. Although a small fraction of CLN7 is present at the plasma membrane [15], it is unlikely that CLN7 exerts its function at the cell surface and that lysosomal targeting and subsequent degradation serve a regulatory function by inactivating the polypeptide. The CLN7 protein has been identified in proteomic analyses of purified lysosomal membranes [2,3] and mutations in the *CLN7*/*MFSD8* gene result in a severe lysosomal storage disorder suggesting an important role of CLN7 for lysosomal biogenesis and function. Interestingly, the promoter region of the *CLN7*/*MFSD8* gene contains the consensus sequence for recognition by the transcription factor TFEB, which is important for lysosomal biogenesis [30,31]. We therefore assume that CLN7 is a *bona fide* lysosomal membrane protein and not a plasma membrane protein.

Proteolytic cleavage of integral lysosomal membrane proteins has been described as a regulatory event to modulate their biological activity. For example, the polytopic lysosomal membrane protein heparin sulfate acetyl-CoA α-glucosaminide N-acetyltransferase (HGSNAT) is synthesized as an catalytically inactive 77 kDa precursor which is partially cleaved in lysosomes into a 29 kDa N-terminal α- and a 48 kDa C-terminal β-chain [32]. It was shown that proteolytic cleavage and intralysosomal oligomerization of HGSNAT are required for functional activation. Similar to CLN7, the HGSNAT precursor is not completely processed and is still present even after extended chase times of 48 and 72 h. Limited proteolytic cleavage in lysosomes has also been reported for the lysosomal membrane proteins LAPTM4a, LAPTM4b and LAPTM5 [33]. The partial cleavage of HGSNAT, LAPTMs and CLN7

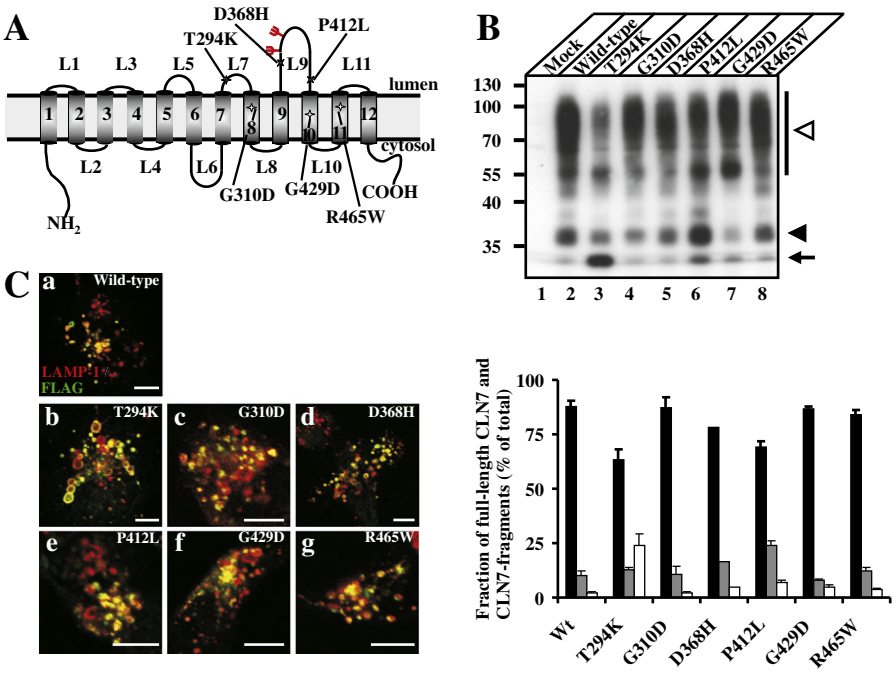

Fig. 8. CLN7 mutations p.T294K and p.P412L alter the proteolytic cleavage of CLN7. (A) Predicted topology model of CLN7 indicating the analyzed missense mutations located in luminal (black stars) and transmembrane domains (white stars). (B) COS-7 cells were mock-transfected (lane 1), transfected with wild-type (lane 2) or mutant 3xFLAG-CLN7 cDNAs (lanes 3–8) and total cell extracts (10 μg) were separated by SDS-PAGE and analyzed by FLAG immunoblotting. Positions of full-length CLN7 (open arrowhead), the N-terminal 36 kDa fragment (closed arrowhead) and an additional band at 33 kDa (arrow) are indicated. Intensities of immunoreactive bands were quantified densitometrically and the mean fractions ± standard deviation of full-length CLN7 (black bar), the 36 kDa (gray bar) and 33 kDa (white bar) CLN7 fragments are shown in a diagram. (C) COS-7 cells were transfected with wild-type (a) and mutant 3xFLAG-CLN7 cDNAs (b-g), fixed and incubated with polyclonal antibodies against FLAG and monoclonal antibodies against the lysosomal membrane protein LAMP-1. 3xFLAG-CLN7 was visualized by anti-rabbit IgG coupled to AlexaFluor 488 (green) and LAMP-1 was visualized by anti-mouse IgG coupled to AlexaFluor 546 (red). Merged images indicate co-localization (yellow). Scale bars, 10 μm.

in lysosomes differs from other lysosomal proteins, where the majority of enzymatically inactive precursors is rapidly converted into mature forms upon arrival in lysosomes as described for most of the soluble lysosomal enzymes and for the lysosomal membrane protein lysosomal acid phosphatase (LAP). LAP is cleaved twice to release its catalytically active soluble form into the lysosomal lumen [34,35]. Another example is mucolipin-1 (ML1), a member of the transient receptor potential superfamily, which is deficient in mucolipidosis type IV [36]. Cleavage of ML1 in the lumenal loop between transmembrane domains 1 and 2 results in two fragments of approximately 37 kDa and 40 kDa [37]. Kiselyov and co-workers demonstrated that ML1 is functionally inactivated by Ctsb-mediated cleavage [37].

We first tested the possibility that proteolytic cleavage of CLN7 is mediated by the ubiquitously expressed cysteine protease Ctsl, which is localized in the lumen of lysosomes and therefore a suitable candidate protease for cleaving sequences localized in lumenal loop L9 of CLN7 [38]. Treatment of COS-7 cells with increasing concentrations of the cathepsin L inhibitors SID26681509 and Z-FY-CHO revealed that cathepsin L is involved in the cleavage generating the 36 kDa fragment. In contrast, formation of the 38 kDa fragment could not be significantly inhibited by SID26681509 even at high concentrations (50 μM), but was reduced in a dose-dependent manner by Z-FY-CHO. However, Z-FY-CHO treatment has a greater inhibitory effect on generation of the 36 kDa fragment than on formation of the 38 kDa fragment (Fig. 4). Z-FY-CHO has a half maximal inhibitory concentration (IC50) of 0.085 μM for cathepsin B [27] and is therefore likely to non-specifically decrease the generation of the 38 kDa fragment by inhibiting other cathepsins such as cathepsin B. To confirm the role of Ctsl for cleavage of CLN7 by an independent approach, expression analyses of CLN7 were performed in *Ctsb*- and *Ctsl*-deficient MEF. CLN7 was still cleaved in $Ctsb^{(-/-)}$ MEF, whereas in $Ctsl^{(-/-)}$ MEF no cleavage to the 36 kDa fragment was observed (Fig. 5). In contrast, the 38 kDa fragment was generated in both wild-type and $Ctsl^{(-/-)}$ MEF. Furthermore, proteolytic cleavage of CLN7 in the $Ctsl^{(-/-)}$ MEF could be rescued by overexpression of Ctsl, but not by overexpression of Ctsb. Phenotypic analyses of single and double deficient mice ($Ctsl/b^{(-/-)}$) have shown that Ctsb and Ctsl can compensate for each other in vivo [38,39]. Our data suggest that Ctsl is critically involved in the cleavage event generating the 36 kDa fragment and that the absence of Ctsl in MEF cannot be complemented by Ctsb. The presence of the 38 kDa fragment in $Ctsl^{(-/-)}$ MEF in combination with the partial inhibition of its generation by Z-FY-CHO, most likely by non-specific inhibition of other lysosomal cysteine proteases, suggests that the cleavage event generating the 38 kDa fragment is independent of Ctsl.

To date, 84 different cysteine proteases are known [40], 11 of which are lysosomal papain-like cysteine cathepsins [41]. Ctsl is one of the major cysteine proteases required for bulk degradation and processing of proteins in lysosomes [42]. Mouse Ctsl represents a well characterized, ubiquitously expressed lysosomal cysteine endopeptidase, which is synthesized as an inactive proenzyme followed by proteolytic cleavage into two chains upon arrival in lysosomes [43]. Analyses of $Ctsl^{(-/-)}$ mice revealed that mouse Ctsl plays a role in the hair cycle [21], epidermal proliferation [21,44], cardiac homeostasis [45], processing of prohormones [46], glucose metabolism [47] and MHCII-mediated antigen presentation [48]. Different substrates of Ctsl have been identified including cytosolic proteins, lysosomal enzyme precursors, nuclear proteins, prohormones and proteins of the extracellular matrix [40]. In addition, the membrane protein Toll-like receptor 9 (TLR9) is proteolytically cleaved by Ctsl in lysosomes upon pathogen exposure releasing a C-terminal fragment which is required for TLR9 signaling [49,50].

Mouse and human cells show different cathepsin expression patterns so one must be cautious with directly relating these findings in mice to processing in human cells. Most notably, the human genome encodes for two cathepsin L proteases, namely cathepsin L1 and cathepsin V, which is also named cathepsin L2 [38,51]. In addition, there are

differences in the abundance of the individual cathepsins among human and mouse cell types, but in our experience both cathepsin L and cathepsin B are generally highly-expressed in mouse MEF. We found that cathepsin L plays a role in CLN7 cleavage in primary mouse embryonic fibroblasts and in the COS-7 monkey fibroblast cell line, indicating that the mechanism of CLN7 cleavage is conserved from mice to primates.

The neuronal ceroid lipofuscinoses are characterized by the accumulation of autofluorescent storage material in lysosomes as well as selective damage and loss of photoreceptors in the retina and neurons in selected regions of the brain [5,52]. However, *Ctsl* deficiency in mice is not associated with these pathological alterations. The phenotype of these mice suggests that Ctsl-mediated proteolytic cleavage is not critically required for the functional activation of CLN7 or that another protease with redundant functions cleaves CLN7 in neuronal cells. Interestingly, mice that are deficient for both Ctsb and Ctsl have a typical NCL-like phenotype with lysosomal storage, loss of neuronal cells and brain atrophy indicating that the presence of both proteases is essential for lysosomal function and maintenance of the central nervous system [39,53,54]. Proteolytic cleavage of CLN7 is presumably reduced in these mice and CLN7 activity enhanced if cleavage inactivates the polypeptide (see below).

A direct comparison of the phenotypes of *Ctsl*/*b*$^{(-/-)}$ and *Cln7*$^{(-/-)}$ mice is not possible as no mouse models for CLN7 disease have been generated so far [14]. However existing mouse models of variant late infantile NCLs (vLINCL; Cln5, Cln6, Cln8) have a later disease onset as compared to *Ctsl*/*b*$^{(-/-)}$ mice which display an early onset and rapid progression of neurodegeneration with death at the age of 2 to 4 weeks [39,52]. The different phenotypes of the vLINCL mouse models make it unlikely that the neurodegenerative phenotype in *Ctsl*/*b*$^{(-/-)}$ mice is caused by impairment of CLN7 function. One possibility is that the deficiency of the redundant cathepsins B and L results in impaired lysosomal proteolysis and protein turnover. This hypothesis would be strengthened by the severe neurodegenerative phenotype of the Cln10 mouse model deficient in the aspartyl protease cathepsin D, which mediates protein degradation and activates precursor forms of proteases [55].

Disease-causing mutations in polytopic lysosomal membrane proteins, such as CLN3 and HGSNAT, are typically retained in the endoplasmic reticulum due to misfolding of the proteins [56,57]. However, we and others have shown that several disease-causing mutations in the *CLN7*/*MFSD8* gene did not alter subcellular localization of CLN7 in lysosomal compartments [9,16], suggesting that these mutations cause alterations in protein stability and/or biological function in lysosomes, rather than retention of misfolded CLN7 proteins in the endoplasmic reticulum or intracellular missorting. In order to study the effect of CLN7 mutations on proteolytic cleavage of CLN7, we expressed both wild-type and mutant CLN7 in COS-7 cells and performed Western blot analyses. We selected mutations localized in lumenal loop L7 (p.T294K), in lumenal loop L9 (p.D368H and p.P412L) or in the transmembrane domains TM8 (p.G310D), TM10 (p.G429D) and TM11 (p.R465W) of CLN7. Both mutations located in lumenal loops (p.T294K and p.P412L) but none of the studied mutations located in transmembrane domains altered Ctsl-mediated proteolytic cleavage (Fig. 8). These results suggest that selected mutations in lumenal loop L9 or in the adjacent lumenal loop L7 alter their conformation rendering them more sensitive to cleavage.

With one exception, the similar clinical phenotype of CLN7 patients suggests that all *CLN7*/*MFSD8* mutations result in a complete loss of CLN7 function [12]. The disease-associated c.103 C>T (p. Arg35X) mutation causes a truncation of CLN7 after the first 34 amino acids with deletion of all 12 transmembrane domains presumably resulting in a non-functional protein [11,12]. The clinical manifestation of patients carrying this mutation is indistinguishable from patients with the p.T294K and p.P412L mutations, strongly suggesting that these mutations also lead to a complete loss of CLN7 function. It is therefore conceivable that enhanced CLN7 proteolysis of p.T294K and p.P412L contributes to CLN7 disease. In this case unprocessed CLN7 would be the functional protein and proteolytic cleavage would inactivate the protein. The observation that only a fraction (56.8% for both cleavage events combined) of CLN7 is proteolytically cleaved strengthens the hypothesis that proteolysis inactivates CLN7, possibly providing a regulatory mechanism to limit the duration of its putative transporter activity.

Although the precise function of CLN7 is unknown its lysosomal localization and its homologies to the MFS family of transporters suggest that it represents a lysosomal transporter. Thus, CLN7 disease can be categorized into the group of lysosomal storage diseases caused by deficiencies of lysosomal transporters [4]. As in other NCLs, the storage material in CLN7 disease contains high amounts of mitochondrial ATP synthase subunit c [58]. It is unknown whether low molecular weight metabolites accumulate in lysosomes and therefore no conclusions can be drawn on the nature of transported CLN7 substrate(s). Sequence comparisons revealed that CLN7 has homologies with amino acid, lactate, pyruvate, glycerophosphoinositol and hexose transporters in yeast. Two of these CLN7 homologues, YCR023C and YBR241C, are localized in vacuolar membranes [59]. Thus, it is possible that accumulation of monosaccharides, carbohydrate derivatives or amino acids in lysosomes due to the deficiency of CLN7 may lead to an NCL-like phenotype in patients. Interestingly, loss of the predicted lysosomal MFS anion/sugar permease *benchwarmer* in *Drosophila melanogaster*, results in an NCL-like phenotype in flies [60]. Furthermore, mutations in the MFS transporter sialin, which exports sialic acid from lysosomes into the cytosol, lead to a lysosomal storage disorder [61].

In summary our data suggest that increased proteolytic cleavage of CLN7 resulting from mutations in luminal loops may lead to impaired function of CLN7 in lysosomes. In addition, the analyzed mutations affecting the sequence of transmembrane domains in CLN7 did not alter proteolytic cleavage of CLN7 in lysosomes suggesting functional impairment by other mechanisms.

Supplementary materials related to this article can be found online at http://dx.doi.org/10.1016/j.bbadis.2012.05.015.

Acknowledgements

This work was supported by the German Research Foundation (GRK1459 to P.S., S. S.). We thank Neele Schumacher for the excellent technical assistance and Dr. Braulke for the critical review of the manuscript. The cDNAs encoding mouse Ctsb and Ctsl and the pcDNA3.1 Hygro (+)-DIRC2-3xMyc expression vector were a kind gift from Dr. Schröder (University of Kiel, Germany). The polyclonal anti-cathepsin D antibody was generously provided by Dr. Hasilik (University of Marburg, Germany).

References

[1] P. Saftig, J. Klumperman, Lysosome biogenesis and lysosomal membrane proteins: trafficking meets function, Nat. Rev. Mol. Cell Biol. 10 (2009) 623–635.
[2] R.D. Bagshaw, D.J. Mahuran, J.W. Callahan, A proteomic analysis of lysosomal integral membrane proteins reveals the diverse composition of the organelle, Mol. Cell. Proteomics 4 (2005) 133–143.
[3] B. Schröder, C. Wrocklage, C. Pan, R. Jager, B. Kösters, H. Schäfer, H.P. Elsässer, M. Mann, A. Hasilik, Integral and associated lysosomal membrane proteins, Traffic 8 (2007) 1676–1686.
[4] R. Ruivo, C. Anne, C. Sagne, B. Gasnier, Molecular and cellular basis of lysosomal transmembrane protein dysfunction, Biochim. Biophys. Acta 1793 (2009) 636–649.
[5] A. Jalanko, T. Braulke, Neuronal ceroid lipofuscinoses, Biochim. Biophys. Acta 1793 (2009) 697–709.
[6] B.A. Benitez, D. Alvarado, Y. Cai, K. Mayo, S. Chakraverty, J. Norton, J.C. Morris, M.S. Sands, A. Goate, C. Cruchaga, Exome-sequencing confirms dnajc5 mutations as cause of adult neuronal ceroid-lipofuscinosis, PLoS One 6 (2011) e26741.
[7] L. Nosková, V. Stránecký, H. Hartmannová, A. Přistoupilová, V. Barešová, R. Ivanek, H. Hůlková, H. Jahnová, J. van der Zee, J.F. Staropoli, K.B. Sims, J. Tyynelä, C. Van Broeckhoven, P.C. Nijssen, S.E. Mole, M. Elleder, S. Kmoch, Mutations in DNAJC5, encoding cysteine-string protein alpha, cause autosomal-dominant adult-onset neuronal ceroid lipofuscinosis, Am. J. Hum. Genet. 89 (2011) 241–252.

[8] J. Bras, A. Verloes, S.A. Schneider, S.E. Mole, R.J. Guerreiro, Mutation of the parkinsonism gene ATP13A2 causes neuronal ceroid-lipofuscinosis, Hum. Mol. Genet. 21 (2012) 2646–2650.
[9] E. Siintola, M. Topcu, N. Aula, H. Lohi, B.A. Minassian, A.D. Paterson, X.Q. Liu, C. Wilson, U. Lahtinen, A.K. Anttonen, A.E. Lehesjoki, The novel neuronal ceroid lipofuscinosis gene MFSD8 encodes a putative lysosomal transporter, Am. J. Hum. Genet. 81 (2007) 136–146.
[10] E. Stogmann, S. El Tawil, J. Wagenstaller, A. Gaber, S. Edris, A. Abdelhady, E. Assem-Hilger, F. Leutmezer, S. Bonelli, C. Baumgartner, F. Zimprich, T.M. Strom, A. Zimprich, A novel mutation in the MFSD8 gene in late infantile neuronal ceroid lipofuscinosis, Neurogenetics 10 (2009) 73–77.
[11] C. Aiello, A. Terracciano, A. Simonati, G. Discepoli, N. Cannelli, D. Claps, Y.J. Crow, M. Bianchi, C. Kitzmüller, D. Longo, A. Tavoni, E. Franzoni, A. Tessa, E. Veneselli, R. Boldrini, M. Filocamo, R.E. Williams, E.S. Bertini, R. Biancheri, R. Carrozzo, S.E. Mole, F.M. Santorelli, Mutations in MFSD8/CLN7 are a frequent cause of variant-late infantile neuronal ceroid lipofuscinosis, Hum. Mutat. 30 (2009) E530–E540.
[12] M. Kousi, E. Siintola, L. Dvorakova, H. Vlaskova, J. Turnbull, M. Topcu, D. Yuksel, S. Gokben, B.A. Minassian, M. Elleder, S.E. Mole, A.E. Lehesjoki, Mutations in CLN7/MFSD8 are a common cause of variant late-infantile neuronal ceroid lipofuscinosis, Brain 132 (2009) 810–819.
[13] M.A. Aldahmesh, Z.N. Al-Hassnan, M. Aldosari, F.S. Alkuraya, Neuronal ceroid lipofuscinosis caused by MFSD8 mutations: a common theme emerging, Neurogenetics 10 (2009) 307–311.
[14] M. Kousi, A.E. Lehesjoki, S.E. Mole, Update of the mutation spectrum and clinical correlations of over 360 mutations in eight genes that underlie the neuronal ceroid lipofuscinoses, Hum. Mutat. 33 (2012) 42–63.
[15] P. Steenhuis, S. Herder, S. Gelis, T. Braulke, S. Storch, Lysosomal targeting of the CLN7 membrane glycoprotein and transport via the plasma membrane require a dileucine motif, Traffic 11 (2010) 987–1000.
[16] A. Sharifi, M. Kousi, C. Sagne, G.C. Bellenchi, L. Morel, M. Darmon, H. Hulkova, R. Ruivo, C. Debacker, S. El Mestikawy, M. Elleder, A.E. Lehesjoki, A. Jalanko, B. Gasnier, A. Kyttälä, Expression and lysosomal targeting of CLN7, a major facilitator superfamily transporter associated with variant late-infantile neuronal ceroid lipofuscinosis, Hum. Mol. Genet. 19 (2010) 4497–4514.
[17] S.S. Pao, I.T. Paulsen, M.H. Saier Jr., Major facilitator superfamily, Microbiol. Mol. Biol. Rev. 62 (1998) 1–34.
[18] M. Hentze, A. Hasilik, K. von Figura, Enhanced degradation of cathepsin D synthesized in the presence of the threonine analog beta-hydroxynorvaline, Arch. Biochem. Biophys. 230 (1984) 375–382.
[19] L.R. Savalas, B. Gasnier, M. Damme, T. Lübke, C. Wrocklage, C. Debacker, A. Jezegou, T. Reinheckel, A. Hasilik, P. Saftig, B. Schröder, Disrupted in renal carcinoma 2 (DIRC2), a novel transporter of the lysosomal membrane, is proteolytically processed by cathepsin L, Biochem. J. 439 (2011) 113–128.
[20] W. Halangk, M.M. Lerch, B. Brandt-Nedelev, W. Roth, M. Ruthenbuerger, T. Reinheckel, W. Domschke, H. Lippert, C. Peters, J. Deussing, Role of cathepsin B in intracellular trypsinogen activation and the onset of acute pancreatitis, J. Clin. Invest. 106 (2000) 773–781.
[21] W. Roth, J. Deussing, V.A. Botchkarev, M. Pauly-Evers, P. Saftig, A. Hafner, P. Schmidt, W. Schmahl, J. Scherer, I. Anton-Lamprecht, K. von Figura, R. Paus, C. Peters, Cathepsin L deficiency as molecular defect of furless: hyperproliferation of keratinocytes and pertubation of hair follicle cycling, FASEB J. 14 (2000) 2075–2086.
[22] A.J. Barrett, A.A. Kembhavi, M.A. Brown, H. Kirschke, C.G. Knight, M. Tamai, K. Hanada, L-trans-epoxysuccinyl-leucylamido(4-guanidino)butane (E-64) and its analogues as inhibitors of cysteine proteinases including cathepsins B, H and L, Biochem. J. 201 (1982) 189–198.
[23] A. Baici, M. Gyger-Marazzi, The slow, tight-binding inhibition of cathepsin B by leupeptin. A hysteretic effect, Eur. J. Biochem. 129 (1982) 33–41.
[24] J.T. Woo, K. Yamaguchi, T. Hayama, T. Kobori, S. Sigeizumi, K. Sugimoto, K. Kondo, T. Tsuji, Y. Ohba, K. Tagami, K. Sumitani, Suppressive effect of N-(benzyloxycarbonyl)-L-phenylalanyl-L-tyrosinal on bone resorption in vitro and in vivo, Eur. J. Pharmacol. 300 (1996) 131–135.
[25] J. Lippincott-Schwartz, L.C. Yuan, J.S. Bonifacino, R.D. Klausner, Rapid redistribution of Golgi proteins into the ER in cells treated with brefeldin A: evidence for membrane cycling from Golgi to ER, Cell 56 (1989) 801–813.
[26] P.P. Shah, M.C. Myers, M.P. Beavers, J.E. Purvis, H. Jing, H.J. Grieser, E.R. Sharlow, A.D. Napper, D.M. Huryn, B.S. Cooperman, A.B. Smith 3rd, S.L. Diamond, Kinetic characterization and molecular docking of a novel, potent, and selective slow-binding inhibitor of human cathepsin L, Mol. Pharmacol. 74 (2008) 34–41.
[27] J.-T. Woo, S. Sigeizumi, K. Yamaguchi, K. Sugimoto, T. Kobori, T. Tsuji, K. Kondo, Peptidyl aldehyde derivatives as potent and selective inhibitors of cathepsin L, Bioorg. Med. Chem. Lett. 5 (1995) 1501–1504.
[28] R. Kundra, S. Kornfeld, Asparagine-linked oligosaccharides protect LAMP-1 and LAMP-2 from intracellular proteolysis, J. Biol. Chem. 274 (1999) 31039–31046.
[29] C.J. Law, P.C. Maloney, D.N. Wang, Ins and outs of major facilitator superfamily antiporters, Annu. Rev. Microbiol. 62 (2008) 289–305.
[30] M. Palmieri, S. Impey, H. Kang, A. di Ronza, C. Pelz, M. Sardiello, A. Ballabio, Characterization of the CLEAR network reveals an integrated control of cellular clearance pathways, Hum. Mol. Genet. 20 (2011) 3852–3866.
[31] M. Sardiello, M. Palmieri, A. di Ronza, D.L. Medina, M. Valenza, V.A. Gennarino, C. Di Malta, F. Donaudy, V. Embrione, R.S. Polishchuk, S. Banfi, G. Parenti, E. Cattaneo, A. Ballabio, A gene network regulating lysosomal biogenesis and function, Science 325 (2009) 473–477.
[32] S. Durand, M. Feldhammer, E. Bonneil, P. Thibault, A.V. Pshezhetsky, Analysis of the biogenesis of heparan sulfate acetyl-CoA:alpha-glucosaminide N-acetyltransferase provides insights into the mechanism underlying its complete deficiency in mucopolysaccharidosis IIIC, J. Biol. Chem. 285 (2010) 31233–31242.
[33] S. Vergarajauregui, J.A. Martina, R. Puertollano, LAPTMs regulate lysosomal function and interact with mucolipin 1: new clues for understanding mucolipidosis type IV, J. Cell Sci. 124 (2011) 459–468.
[34] S. Gottschalk, A. Waheed, B. Schmidt, P. Laidler, K. von Figura, Sequential processing of lysosomal acid phosphatase by a cytoplasmic thiol proteinase and a lysosomal aspartyl proteinase, EMBO J. 8 (1989) 3215–3219.
[35] A. Waheed, S. Gottschalk, A. Hille, C. Krentler, R. Pohlmann, T. Braulke, H. Hauser, H. Geuze, K. von Figura, Human lysosomal acid phosphatase is transported as a transmembrane protein to lysosomes in transfected baby hamster kidney cells, EMBO J. 7 (1988) 2351–2358.
[36] D.A. Zeevi, A. Frumkin, G. Bach, TRPML and lysosomal function, Biochim. Biophys. Acta 1772 (2007) 851–858.
[37] K. Kiselyov, J. Chen, Y. Rbaibi, D. Oberdick, S. Tjon-Kon-Sang, N. Shcheynikov, S. Muallem, A. Soyombo, TRP-ML1 is a lysosomal monovalent cation channel that undergoes proteolytic cleavage, J. Biol. Chem. 280 (2005) 43218–43223.
[38] J. Reiser, B. Adair, T. Reinheckel, Specialized roles for cysteine cathepsins in health and disease, J. Clin. Invest. 120 (2010) 3421–3431.
[39] U. Felbor, B. Kessler, W. Mothes, H.H. Goebel, H.L. Ploegh, R.T. Bronson, B.R. Olsen, Neuronal loss and brain atrophy in mice lacking cathepsins B and L, Proc. Natl. Acad. Sci. U. S. A. 99 (2002) 7883–7888.
[40] N.D. Rawlings, A.J. Barrett, A. Bateman, MEROPS: the peptidase database, Nucleic Acids Res. 38 (2010) D227–D233.
[41] B. Turk, D. Turk, V. Turk, Lysosomal cysteine proteases: more than scavengers, Biochim. Biophys. Acta 1477 (2000) 98–111.
[42] K. Brix, A. Dunkhorst, K. Mayer, S. Jordans, Cysteine cathepsins: cellular roadmap to different functions, Biochimie 90 (2008) 194–207.
[43] K. Ishidoh, E. Kominami, Processing and activation of lysosomal proteinases, Biol. Chem. 383 (2002) 1827–1831.
[44] T. Reinheckel, S. Hagemann, S. Dollwet-Mack, E. Martinez, T. Lohmüller, G. Zlatkovic, D.J. Tobin, N. Maas-Szabowski, C. Peters, The lysosomal cysteine protease cathepsin L regulates keratinocyte proliferation by control of growth factor recycling, J. Cell Sci. 118 (2005) 3387–3395.
[45] J. Stypmann, K. Glaser, W. Roth, D.J. Tobin, I. Petermann, R. Matthias, G. Monnig, W. Haverkamp, G. Breithardt, W. Schmahl, C. Peters, T. Reinheckel, Dilated cardiomyopathy in mice deficient for the lysosomal cysteine peptidase cathepsin L, Proc. Natl. Acad. Sci. U. S. A. 99 (2002) 6234–6239.
[46] L. Funkelstein, T. Toneff, C. Mosier, S.R. Hwang, F. Beuschlein, U.D. Lichtenauer, T. Reinheckel, C. Peters, V. Hook, Major role of cathepsin L for producing the peptide hormones ACTH, beta-endorphin, and alpha-MSH, illustrated by protease gene knockout and expression, J. Biol. Chem. 283 (2008) 35652–35659.
[47] M. Yang, Y. Zhang, J. Pan, J. Sun, J. Liu, P. Libby, G.K. Sukhova, A. Doria, N. Katunuma, O.D. Peroni, M. Guerre-Millo, B.B. Kahn, K. Clement, G.P. Shi, Cathepsin L activity controls adipogenesis and glucose tolerance, Nat. Cell Biol. 9 (2007) 970–977.
[48] T. Nakagawa, W. Roth, P. Wong, A. Nelson, A. Farr, J. Deussing, J.A. Villadangos, H. Ploegh, C. Peters, A.Y. Rudensky, Cathepsin L: critical role in Ii degradation and CD4 T cell selection in the thymus, Science 280 (1998) 450–453.
[49] B. Park, M.M. Brinkmann, E. Spooner, C.C. Lee, Y.M. Kim, H.L. Ploegh, Proteolytic cleavage in an endolysosomal compartment is required for activation of Toll-like receptor 9, Nat. Immunol. 9 (2008) 1407–1414.
[50] K. Takeda, T. Kaisho, S. Akira, Toll-like receptors, Annu. Rev. Immunol. 21 (2003) 335–376.
[51] D. Brömme, V. Cathepsin, in: A.J. Barrett, J.F. Woessner (Eds.), Handbook of Proteolytic Enzymes, Elsevier, London, 2004, p. 1107.
[52] J.D. Cooper, C. Russell, H.M. Mitchison, Progress towards understanding disease mechanisms in small vertebrate models of neuronal ceroid lipofuscinosis, Biochim. Biophys. Acta 1762 (2006) 873–889.
[53] M. Koike, M. Shibata, S. Waguri, K. Yoshimura, I. Tanida, E. Kominami, T. Gotow, C. Peters, K. von Figura, N. Mizushima, P. Saftig, Y. Uchiyama, Participation of autophagy in storage of lysosomes in neurons from mouse models of neuronal ceroid-lipofuscinoses (Batten disease), Am. J. Pathol. 167 (2005) 1713–1728.
[54] L. Sevenich, L.A. Pennacchio, C. Peters, T. Reinheckel, Human cathepsin L rescues the neurodegeneration and lethality in cathepsin B/L double-deficient mice, Biol. Chem. 387 (2006) 885–891.
[55] M. Koike, H. Nakanishi, P. Saftig, J. Ezaki, K. Isahara, Y. Ohsawa, W. Schulz-Schaeffer, T. Watanabe, S. Waguri, S. Kametaka, M. Shibata, K. Yamamoto, E. Kominami, C. Peters, K. von Figura, Y. Uchiyama, Cathepsin D deficiency induces lysosomal storage with ceroid lipofuscin in mouse CNS neurons, J. Neurosci. 20 (2000) 6898–6906.
[56] M. Feldhammer, S. Durand, A.V. Pshezhetsky, Protein misfolding as an underlying molecular defect in mucopolysaccharidosis III type C, PLoS One 4 (2009) e7434.
[57] I. Jarvelä, M. Lehtovirta, R. Tikkanen, A. Kyttälä, A. Jalanko, Defective intracellular transport of CLN3 is the molecular basis of Batten disease (JNCL), Hum. Mol. Genet. 8 (1999) 1091–1098.
[58] S. Mole, R. Williams, H. Goebel, The Neuronal Ceroid Lipofuscinoses (Batten Disease), Oxford University Press, UK, 2011.
[59] E. Wiederhold, T. Gandhi, H.P. Permentier, R. Breitling, B. Poolman, D.J. Slotboom, The yeast vacuolar membrane proteome, Mol. Cell. Proteomics 8 (2009) 380–392.
[60] B. Dermaut, K.K. Norga, A. Kania, P. Verstreken, H. Pan, Y. Zhou, P. Callaerts, H.J. Bellen, Aberrant lysosomal carbohydrate storage accompanies endocytic defects and neurodegeneration in Drosophila benchwarmer, J. Cell Biol. 170 (2005) 127–139.
[61] F.W. Verheijen, E. Verbeek, N. Aula, C.E. Beerens, A.C. Havelaar, M. Joosse, L. Peltonen, P. Aula, H. Galjaard, P.J. van der Spek, G.M. Mancini, A new gene, encoding an anion transporter, is mutated in sialic acid storage diseases, Nat. Genet. 23 (1999) 462–465.